2H-[1,2,3]Triazolo[4,5-c]pyridine Cored Organic Dyes Achieving a High Efficiency: a Systematic Study of the Effect of Different Donors and π Spacers

Sumit Chaurasia,[†] Jen-Shyang Ni,[†] Wei-I Hung, and Jiann T. Lin*

Institute of Chemistry, Academia Sinica, Nankang, Taipei 115, Taiwan

S *Supporting Information*

ABSTRACT: New D−A−π−A-based isomeric sensitizers, **PTN**n (n = 1−2) and **NPT**n (n = 1−5), were synthesized using 2H-[1,2,3]triazolo[4,5-c]pyridine (**PT**) as an auxiliary acceptor, triphenylamine or N,N-bis[4-(hexyloxy)phenyl]-aniline as the donor, furan, thiophene, phenyl, or 3-hexylthiophene as the conjugated spacer, and 2-cyanoacrylic acid as the acceptor and anchor as well. They were used as the sensitizers of dye-sensitized solar cells. The **NPT**n dyes show better performance than the **PTN**n dyes. Among them, the best efficiency of 7.92% (∼96%, **N719**) was obtained with the **NPT5** dye, indicating that the **PT** core could be used as a new building block for the design of high-performance sensitizers in the future. The negative Mulliken charge from the auxiliary acceptor was found to be useful as a semiempirical index for correlation of the molecular structure with the cell efficiency among structurally similar D−A−π−A-type congeners.

J_{sc} = 14.90 mA/cm^2
V_{oc} = 0.72 V
η = 7.92%

KEYWORDS: 2H-[1,2,3]triazolo[4,5-c]pyridine, Mulliken charges, donor−acceptor−acceptor systems, metal-free sensitizers, dye-sensitized solar cells
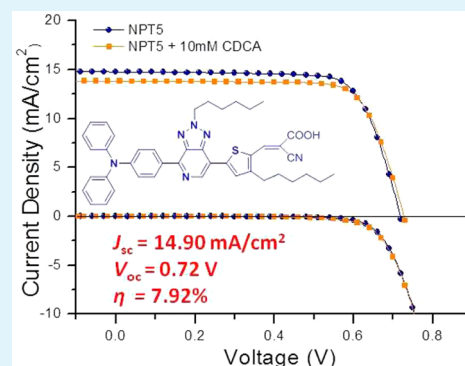
1. INTRODUCTION

The thrust to harvest solar light as a source of renewable energy in the form of dye-sensitized solar cells (DSSCs)[1−3] has made significant progress after the pioneering work of Grätzel and co-workers on ruthenium complexes,[4] and recently the group achieved a record efficiency (η) of 13.0% based on a zinc porphyrin complex.[5] In comparison, an impressive efficiency of 12.5%[6] was also obtained with metal-free sensitizers. In recent years, metal-free dyes receive increasing attention because of their design flexibility and low production cost.[7−15] A conventional metal-free dye has a common structural motif of D−π−A,[16−21] where D is the electron donor, A is the electron acceptor, and π is the conjugated spacer between the two. The individual units such as donor and π-conjugated spacer along with the acceptor/anchoring group are important for the design of organic dyes. Usually the photovoltaic performance of the organic dye can easily be tuned by judicious modification of these individual units, which can easily be done by using different donor groups, such as the recent exploration of carbazole/benzocarbazole[22,23] and fluorenylamine[24] by Han et al. and π-conjugated spacers such as thiophene, furan, and benzene.[25] Intramolecular charge-transfer (ICT) transition from the donor to the acceptor is normally responsible for electron injection from the photoexcited dye molecule to the TiO$_2$ conduction band.

We previously found that insertion of an electron-deficient entity, benzothiadiazole (**BT**), as the extra auxiliary acceptor in the conjugated spacer of the D−π−A molecule,[26] now known as the D−A−π−A type,[27−30] was an efficient way to red shift the ICT band. Judicious selection of the donor and conjugated spacer was demonstrated to be important for high-performance of DSSCs, however. More recently, we applied the concept of D−A−π−A using pyrido[2,1,3]thiadiazole (**PyT**),[31] a more electron-deficient entity than **BT**, as the second electron acceptor. Disappointingly, the **PyT** dyes exhibited lower cell performance than the **BT** congener in spite of the more red shift of the ICT band. In comparison, replacement of **BT** by a less electron-deficient benzotriazole (**BTA**) entity was found to improve the cell performance although the **BTA** dye exhibited a blue shift of the ICT band.[32−34] With this encouragement, we extended our study to the 2H-[1,2,3]triazolo[4,5-c]pyridine (**PT**) entity. In a recent communication, we reported two isomeric **PT**-based dyes, **PTN1** with the N atom facing toward the acceptor and **NPT1** with the N atom facing away from the acceptor, and found that the latter had a better cell performance. Moreover, **NPT1** had a conversion efficiency nearly 1 order higher than that of the **PT** congener after the addition of chenodeoxycholic acid (CDCA) as the coadsorbent.[35] After developing one more **PTN** dye, we turned our attention to more efficient **NPT** dyes in order to have a better understanding of the molecular structure of the dye versus DSSC performance and to further improve the cell efficiency.

In this study, the physical properties of these dyes and the performance of the DSSCs fabricated will be discussed.

2. EXPERIMENTAL SECTION

2.1. General Information. ^{1}H and ^{13}C NMR spectra were taken on a Bruker AMX-400, AV-400, or AVIII-500 spectrometer using chloroform-d_1 (CDCl$_3$), tetrahydrofuran-d_8, or acetone-d_6 as the solvent. Cyclic voltammetric (CV) measurement was performed on a CHI-621A potentiostat (CH Instruments, Inc.) using CH$_2$Cl$_2$ as the solvent. Ultraviolet−visible (UV−vis) spectra were recorded on a DB-20 spectrophotometer (Dynamica, Inc.). Photoluminescance (fluorescence) spectra were recorded on a F-4500 spectrophotometer (Hitachi, Inc.). Elemental analysis was performed on a PerkinElmer 2400 analyzer. Fast atom bombardment mass spectrometry (FAB MS) analysis was performed on a JEOL Tokyo Japan JMS-700 mass spectrometer equipped with the standard FAB source. The photoelectrochemical characterizations on the solar cells were carried out using an Oriel Class AAA solar simulator (Oriel 94043 A, Newport Corp.). Photocurrent−voltage characteristics of the DSSCs were recorded with a potentiostat/galvanostat (CHI650B, CH Instruments, Inc.) at a light intensity of 100 mW cm^{-2} calibrated by an Oriel reference solar cell (Oriel 91150, Newport Corp.). The monochromatic quantum efficiency was recorded through a monochromator (Oriel 74100, Newport Corp.) at short-circuit conditions. The intensity of each wavelength was in the range of 1−3 mW cm^{-2}. Electrochemical impedance spectroscopy (EIS) spectra were recorded for DSSC under illumination at open-circuit voltage (V_{OC}) at −0.55 V potential at room temperature. The frequencies explored ranged from 10 mHz to 400 kHz. The TiO$_2$ nanoparticles and the reference compound, N719, were purchased from Solaronix, SA, Switzerland.

2.2. Synthesis. *5-(7-Bromo-2-hexyl-2H-[1,2,3]triazolo[4,5-c]-pyridin-4-yl)furan-2-carbaldehyde (3a).* A dry two-neck round-bottomed flask was equipped with a Schlenk adapter and rubber septum. Under nitrogen, a mixture of **1** (362 mg, 1.0 mmol), [5-(1,3-dioxolan-2-yl)furan-2-yl]tributylstannane (**2a**, 516 mg, 1.2 mmol), and PdCl$_2$(PPh$_3$)$_2$ (2% mmol) in the flask was added to dry *N,N*-dimethylformamide (DMF). The reaction was stirred at 100 °C under nitrogen for 16 h. The reaction was monitored through thin-layer chromatography. When the reaction was complete, DMF was removed under high vacuum, and the mixture was poured into deionized water and extracted with dichloromethane (DCM; 3 × 100 mL). The organic phases were collected, washed with deionized water and brine, dried over MgSO$_4$, filtered, and concentrated. The obtained crude product was dissolved in acetic acid and stirred at 50 °C. When a clear solution was obtained, 0.50 mL of water was added, and the solution was stirred overnight. The reaction mixture was cooled and poured into ice water, and the solid obtained was filtered, washed with water several times, and then purified by flash column chromatography using DCM/hexane (3:1) as the eluent to afford **3a** as a light-yellow solid (63%). ^{1}H NMR (300 MHz, CDCl$_3$): δ 0.82−0.86 (m, 3H), 1.26−1.36 (m, 6H), 2.08−2.18 (m, 2H), 4.81 (t, ^3J = 7.38 Hz, 2H), 7.38 (d, ^3J = 3.6 Hz, 1H), 7.76 (d, ^3J = 3.8 Hz, 1H), 8.58 (s, 1H), 9.86 (s, 1H). ^{13}C NMR (75 MHz, CDCl$_3$): δ 14.05, 22.51, 26.28, 30.14, 31.21, 58.05, 108.08, 116.80, 120.33, 138.55, 140.13, 143.93, 147.35, 153.78, 153.88, 179.05. MS (EI): *m/z* 378 (100%), 376 (98%), 318 (17%), 316 (16%), 293 (40%), 291(21%).

5-(7-Bromo-2-hexyl-2H-[1,2,3]triazolo[4,5-c]pyridin-4-yl)-thiophene-2-carbaldehyde (3b). The synthetic procedure was similar to that of **3a**. The crude product was purified by flash chromatography using DCM/hexane (3:1) as the eluent to afford **3b** as a light-yellow solid (71%). ^{1}H NMR (300 MHz, CDCl$_3$): δ 0.82−0.89 (m, 3H), 1.27−1.39 (m, 6H), 2.10−2.22 (m, 2H), 4.82 (t, ^3J = 7.4 Hz, 2H), 7.80 (d, ^3J = 4.0 Hz, 1H), 8.44 (d, ^3J = 4.0 Hz, 1H), 8.48 (s, 1H), 9.95 (s, 1H). ^{13}C NMR (75 MHz, CDCl$_3$): δ 14.10, 22.57, 26.34, 30.20, 31.27, 58.05, 107.68, 130.73, 136.79, 138.72, 143.76, 144.36, 145.58, 147.40, 149.63, 183.46. MS (EI): *m/z* 394 (100%), 392 (95%), 335 (11%), 309 (15%), 282 (12%).

5-[7-[4-(Diphenylamino)phenyl]-2-hexyl-2H-[1,2,3]triazolo[4,5-c]pyridin-4-yl]furan-2-carbaldehyde (5a). Under nitrogen, a mixture

of **3a** (200 mg, 0.53 mmol), *N,N*-diphenyl-4-(tributylstannyl)aniline (**4**, 340 mg, 0.64 mmol), and PdCl$_2$(PPh$_3$)$_2$ (2% mmol) in a flame-dried two-neck flask equipped with a Schlenk adapter and rubber septum was added to dry DMF. The reaction mixture was stirred at 100 °C under nitrogen for 16 h. Upon completion, DMF was removed under high vacuum, and the mixture was poured into deionized water, extracted with DCM/water, dried over MgSO$_4$, filtered, and concentrated. The crude product was purified by flash column chromatography using DCM/hexane (4:1) as the eluent and dried under high vacuum to afford **5a** as a red solid (56%). ^{1}H NMR (300 MHz, CDCl$_3$): δ 0.84−0.90 (m, 3H), 1.27−1.43 (m, 6H), 2.13−2.21 (m, 2H), 4.83 (t, ^3J = 7.3 Hz, 2H), 7.02−7.08 (m, 2H), 7.13−7.21 (m, 6H), 7.25−7.31 (m, 4H), 7.42 (d, ^3J = 3.8 Hz, 1H), 7.80 (d, ^3J = 3.8 Hz, 1H), 7.98 (d, ^3J = 8.7 Hz, 2H), 8.74 (s, 1H), 9.90 (s, 1H). ^{13}C NMR (75 MHz, CDCl$_3$): δ 14.09, 22.55, 26.35, 30.15, 31.26, 57.65, 115.92, 120.42, 122.76, 123.81, 125.30, 125.42, 127.30, 129.43, 129.57, 138.73, 139.05, 139.58, 145.99, 147.34, 148.87, 153.51, 154.91, 179.06. MS (MALDI): *m/z* 541 ([M]$^+$).

5-[7-[4-(Diphenylamino)phenyl]-2-hexyl-2H-[1,2,3]triazolo[4,5-c]pyridin-4-yl]thiophene-2-carbaldehyde (5b). The synthetic procedure was similar to that of **5a**. The crude product was purified by flash chromatography using DCM/hexane (4:1) as the eluent to afford **5b** as a red solid (79%). ^{1}H NMR (300 MHz, CDCl$_3$): δ 0.84−0.90 (m, 3H), 1.27−1.43 (m, 6H), 2.12−2.24 (m, 2H), 4.82 (t, ^3J = 7.3 Hz, 2H), 7.04−7.11 (m, 2H), 7.15−7.21 (m, 6H), 7.25−7.33 (m, 4H), 7.83 (d, ^3J = 4.0 Hz, 1H), 7.98 (d, ^3J = 8.7 Hz, 2H), 8.50 (d, ^3J = 4.0 Hz, 1H), 8.64 (s, 1H), 9.96 (s, 1H). ^{13}C NMR (75 MHz, CDCl$_3$): δ 14.14, 22.61, 26.41, 30.21, 31.32, 57.67, 122.86, 123.83, 125.34, 127.56, 129.37, 129.62, 129.91, 137.06, 139.17, 139.43, 142.95, 144.81, 146.10, 147.44, 148.82, 151.10, 183.47. MS (MALDI): *m/z* 557 ([M]$^+$).

2-Cyano-3-[5-[7-[4-(diphenylamino)phenyl]-2-hexyl-2H-[1,2,3]-triazolo[4,5-c]pyridin-4-yl]furan-2-yl]acrylic Acid (PTN1). A mixture of **5a** (150 mg, 0.28 mmol), cyanoacetic acid (29 mg, 0.34 mmol), ammonium acetate (5 mg), and acetic acid (8 mL) was heated at 100 °C for 3 h. The solution was cooled and poured into crushed ice. After filtration, the solid was washed thoroughly with water and then purified through flash chromatography using 2% acetic acid in DCM. Further recrystallization of the crude product using a mixture of DCM/acetone afforded **PTN1** as a red solid (62%). ^{1}H NMR (400 MHz, THF-d_8): δ 0.85−0.91 (m, 3H), 1.30−1.46 (m, 6H), 2.15−2.24 (m, 2H), 4.92 (t, ^3J = 7.0 Hz, 2H), 7.03−7.09 (m, 2H), 7.13−7.18 (m, 6H), 7.26−7.32 (m, 4H), 7.80 (d, ^3J = 3.8 Hz, 1H), 7.86 (d, ^3J = 3.8 Hz, 1H), 8.15 (d, ^3J = 3.5 Hz, 2H), 8.20 (s, 1H), 8.82 (s, 1H). ^{13}C NMR (100 MHz, THF-d_8): δ 14.44, 23.48, 27.27, 31.04, 32.30, 58.26, 101.55, 116.12, 117.29, 122.58, 123.67, 124.56, 125.73, 126.07, 128.88, 130.39, 139.51, 139.61, 139.89, 140.51, 146.84, 148.59, 149.78, 151.42, 156.77, 163.91. IR (ν_{max}/cm^{-1}, solid): 2922, 2857, 2223, 1695, 1588, 1469, 1328, 1266, 1195, 1025, 983, 836, 807, 752, 696. HRMS (EI). Calcd for C$_{37}$H$_{33}$N$_6$O$_3$ ([M + H]$^+$): *m/z* 609.2614. Found: *m/z* 609.2627.

2-Cyano-3-[5-[7-[4-(diphenylamino)phenyl]-2-hexyl-2H-[1,2,3]-triazolo[4,5-c]pyridin-4-yl]thiophen-2-yl]acrylic Acid (PTN2). The synthetic procedure was similar to that of **PTN1**. The crude product was purified through flash chromatography using 2% acetic acid in DCM and further recrystallized using a mixture of DCM/acetone to afford **PTN2** as a red solid (61%). ^{1}H NMR (400 MHz, acetone-d_6): δ 0.85−0.91 (m, 3H), 1.29−1.49 (m, 6H), 2.11−2.29 (m, 2H), 5.00 (t, ^3J = 7.0 Hz, 2H), 7.14−7.23 (m, 8H), 7.37−7.43 (m, 4H), 8.11 (d, ^3J = 3.5 Hz, 1H), 8.18 (d, ^3J = 8.0 Hz, 2H), 8.53 (s, 1H), 8.61 (d, ^3J = 3.5 Hz, 1H), 8.76 (s, 1H). ^{13}C NMR (100 MHz, acetone-d_6): δ 13.29, 22.18, 25.96, 29.64, 30.95, 57.30, 100.15, 115.77, 122.26, 123.81, 124.86, 125.09, 127.46, 129.36, 129.55, 129.96, 137.92, 138.78, 139.13, 139.82, 142.35, 145.68, 146.49, 147.31, 148.73, 150.56, 162.88. IR (ν_{max}/cm^{-1}, solid): 2920, 2853, 2223, 1702, 1589, 1485, 1268, 1205, 1079, 903, 833, 749, 724, 694. HRMS (EI). Calcd for C$_{37}$H$_{33}$N$_6$O$_2$S ([M + H]$^+$): *m/z* 625.2385. Found: *m/z* 625.2401.

4-(7-Bromo-2-hexyl-2H-[1,2,3]triazolo[4,5-c]pyridin-4-yl)-N,N-di-phenylaniline (7a). The synthetic procedure was similar to that of **5a**. The crude product was purified by flash chromatography using DCM/

hexane (1:1) as the eluent to afford **6a** as a yellow solid (70%). ¹H NMR (300 MHz, CDCl₃): δ 0.84−0.89 (m, 3H), 1.29−1.39 (m, 6H), 2.10−2.19 (m, 2H), 4.79 (t, ³*J* = 7.4 Hz, 2H), 7.04−7.12 (m, 2H), 7.16−7.22 (m, 6H), 7.26−7.33 (m, 4H), 8.48 (d, ³*J* = 8.76 Hz, 2H), 8.52 (s, 1H). ¹³C NMR (75 MHz, CDCl₃): δ 14.09, 22.54, 26.32, 30.18, 31.26, 57.66, 104.92, 122.00, 123.96, 125.51, 129.47, 129.57, 130.16, 139.81, 143.64, 147.26, 147.52, 150.11. MS (MALDI): *m/z* 527 ([M]⁺).

4-[4-Bromo-2-hexyl-2H-[1,2,3]triazolo[4,5-c]pyridin-7-yl)-N,N-bis-(4-(hexyloxy)phenyl]aniline (7b). The synthetic procedure was similar to that of **5a**. The crude product was purified by flash chromatography using DCM/hexane (1:1) as the eluent to afford **7b** as a red solid (67%). ¹H NMR (400 MHz, CDCl₃): δ 0.84−0.94 (m, 9H), 1.27−1.39 (m, 14H), 1.42−1.51 (m, 4H), 1.72−1.81 (m, 4H), 2.10−2.18 (m, 2H), 3.92 (t, ³*J* = 6.5 Hz, 4H), 4.77 (t, ³*J* = 7.3 Hz, 2H), 6.84 (d, ³*J* = 8.84 Hz, 4H), 7.00 (d, ³*J* = 8.92 Hz, 2H), 7.10 (d, ³*J* = 8.84 Hz, 4H), 8.42 (d, ³*J* = 8.88 Hz, 2H), 8.49 (s, 1H). ¹³C NMR (100 MHz, CDCl₃): δ 13.98, 14.10, 22.45, 22.68, 25.83, 26.24, 29.39, 30.08, 31.19, 31.67, 57.50, 68.34, 104.17, 115.45, 118.83, 127.43, 129.99, 139.71, 139.92, 143.56, 147.40, 150.27, 150.94, 156.19. MS (EI): *m/z* 727 (100%), 725 (85%), 642 (35%), 640 (32%), 558 (23%), 556 (22%).

5-[4-]4-(Diphenylamino)phenyl]-2-hexyl-2H-[1,2,3]triazolo[4,5-c]pyridin-7-yl]furan-2-carbaldehyde (8a). The synthetic procedure was similar to that of **3a**. The crude product was purified by flash chromatography using DCM/hexane (4:1) as the eluent to afford **8a** as a red solid in 66% yield. ¹H NMR (300 MHz, CDCl₃): δ 0.86−0.90 (m, 3H), 1.26−1.39 (m, 6H), 2.12−2.19 (m, 2H), 4.79 (t, ³*J* = 7.2 Hz, 2H), 7.04−7.11 (m, 2H), 7.14−7.20 (m, 6H), 7.27−7.31 (m, 4H), 7.38 (d, ³*J* = 3.6 Hz, 1H), 7.53 (d, ³*J* = 3.6 Hz, 1H), 8.57 (d, ³*J* = 8.76 Hz, 2H), 9.01 (s, 1H), 9.71 (s, 1H). MS (FAB): *m/z* 542 ([M + H]⁺).

5-[4-[4-(Diphenylamino)phenyl]-2-hexyl-2H-[1,2,3]triazolo[4,5-c]pyridin-7-yl]thiophene-2-carbaldehyde (8b). The synthetic procedure was similar to that of **3a**. The crude product was purified by flash chromatography using DCM/hexane (4:1) as the eluent to afford **8b** as a red solid in 68% yield. ¹H NMR (400 MHz, CDCl₃): δ 0.84−0.90 (m, 3H), 1.28−1.40 (m, 6H), 2.15−2.22 (m, 2H), 4.81 (t, ³*J* = 7.2 Hz, 2H), 7.05−7.11 (m, 2H), 7.14−7.20 (m, 6H), 7.27−7.32 (m, 4H), 7.785 (d, ³*J* = 3.5 Hz, 1H), 8.065 (d, ³*J* = 3.5 Hz, 1H), 8.56 (d, ³*J* = 8.0 Hz, 2H), 8.82 (s, 1H), 9.92 (s, 1H). ¹³C NMR (75 MHz, CDCl₃): δ 14.13, 22.60, 26.39, 30.16, 31.30, 57.58, 116.22, 121.74, 124.14, 125.68, 127.58, 129.63, 130.42, 137.22, 139.58, 140.12, 143.01, 145.29, 147.19, 147.27, 150.35, 151.18, 182.99. MS (MALDI): *m/z* 557 ([M]⁺).

4-[4-[4-(Diphenylamino)phenyl]-2-hexyl-2H-[1,2,3]triazolo[4,5-c]pyridin-7-yl]benzaldehyde (8c). The synthetic procedure was similar to that of **3a**. The crude product was purified by flash chromatography using DCM/hexane (4:1) as the eluent to afford **8c** as a red solid in 70% yield. ¹H NMR (300 MHz, CDCl₃): δ 0.83−0.89 (m, 3H), 1.29−1.39 (m, 6H), 2.11−2.22 (m, 2H), 4.82 (t, ³*J* = 7.3 Hz, 2H), 7.03−7.11 (m, 2H), 7.16−7.21 (m, 6H), 7.25−7.32 (m, 4H), 8.02 (d, ³*J* = 8.3 Hz, 2H), 8.26 (d, ³*J* = 8.3 Hz, 2H), 8.57 (d, ³*J* = 8.8 Hz, 2H), 8.76 (s, 1H), 10.06 (s, 1H). ¹³C NMR (75 MHz, CDCl₃): δ 14.13, 22.61, 26.40, 30.23, 31.32, 57.52, 121.56, 121.99, 124.03, 125.59, 128.86, 129.62, 129.88, 130.39, 135.82, 139.97, 141.04, 141.29, 146.53, 147.29, 150.19, 151.03, 192.02. MS (MALDI): *m/z* 551 ([M]⁺).

5-[7-[4-[Bis[4-(hexyloxy)phenyl]amino]phenyl]-2-hexyl-2H-[1,2,3]triazolo[4,5-c]pyridin-4-yl]furan-2-carbaldehyde (8d). The synthetic procedure was similar to that of **3a**. The crude product was purified by flash chromatography using DCM/hexane (4:1) as the eluent to afford **8d** as a violet solid (80%). ¹H NMR (500 MHz, CDCl₃): δ 0.84−0.94 (m, 9H), 1.29−1.51 (m, 18H), 1.72−1.81 (m, 4H), 2.10−2.16 (m, 2H), 3.93 (t, ³*J* = 6.4 Hz, 4H), 4.79 (t, ³*J* = 7.2 Hz, 2H), 6.84 (d, ³*J* = 8.75 Hz, 4H), 7.00 (d, ³*J* = 8.85 Hz, 2H), 7.10 (d, ³*J* = 8.70 Hz, 4H), 7.38 (d, ³*J* = 3.5 Hz, 1H), 7.52 (d, ³*J* = 3.5 Hz, 1H), 8.52 (d, ³*J* = 8.80 Hz, 2H), 9.01 (s, 1H), 9.71 (s, 1H). ¹³C NMR (125 MHz, CDCl₃): δ 14.02, 14.11, 22.50, 22.70, 25.86, 26.31, 29.42, 30.05, 31.23, 31.70, 57.37, 68.42, 111.31, 113.18, 115.52, 118.78, 127.54, 127.81, 130.43, 139.42, 139.50, 139.87, 144.48, 151.20, 151.59, 152.21,

154.78, 156.32, 177.50. MS (FAB): *m/z* 742 (100%), 741 (85%), 656 (20%).

2-Cyano-3-[5-[4-[4-(diphenylamino)phenyl]-2-hexyl-2H-[1,2,3]triazolo[4,5-c]pyridin-7-yl]furan-2-yl]acrylic Acid (NPT1). The synthetic procedure was similar to that of **PTN1**. The crude product was purified through flash chromatography using 2% acetic acid in DCM and further recrystallized using a mixture of DCM/acetone to afford **NPT1** as a red solid in 71% yield. ¹H NMR (300 MHz, acetone-*d₆*): δ 0.82−0.89 (m, 3H), 1.27−1.46 (m, 6H), 2.18−2.29 (m, 2H), 4.97 (t, ³*J* = 7.0 Hz, 2H), 7.11−7.16 (m, 2H), 7.17−7.25 (m, 6H), 7.37−7.44 (m, 4H), 7.63 (d, ³*J* = 3.6 Hz, 1H), 7.70 (d, ³*J* = 3.6 Hz, 1H), 8.15 (s, 1H), 8.73 (d, ³*J* = 8.88 Hz, 2H), 9.12 (s, 1H). ¹³C NMR (125 MHz, DMSO-*d₆* + CDCl₃): δ 13.47, 21.71, 25.43, 29.17, 30.39, 56.67, 100.11, 111.08, 114.21, 116.40, 120.45, 123.74, 123.93, 124.98, 128.79, 129.14, 129.80, 136.61, 138.45, 138.54, 143.29, 146.23, 147.90, 149.45, 149.56, 153.01. IR (*ν*ₘₐₓ/cm⁻¹, solid): 2925, 2857, 2222, 1718, 1563, 1490, 1456, 1368, 1294, 1270, 1190, 1163, 1025, 816, 756, 692, 652. HRMS (EI). Calcd for C₃₇H₃₃N₆O₃ ([M + H]⁺): *m/z* 609.2614. Found: *m/z* 609.2628.

2-Cyano-3-[5-[4-[4-(diphenylamino)phenyl]-2-hexyl-2H-[1,2,3]triazolo[4,5-c]pyridin-7-yl]thiophen-2-yl]acrylic Acid (NPT2). The synthetic procedure was similar to that of **PTN1**. The crude product was purified through flash chromatography using 2% acetic acid in DCM and further recrystallized using a mixture of DCM/acetone to afford **NPT2** as a dark-red solid (65%). ¹H NMR (300 MHz, acetone-*d₆*): δ 0.84−0.91 (m, 3H), 1.29−1.47 (m, 6H), 2.23−2.29 (m, 2H), 5.00 (t, ³*J* = 7.0 Hz, 2H), 7.12−7.16 (m, 2H), 7.18−7.25 (m, 6H), 7.38−7.44 (m, 4H), 8.13 (d, ³*J* = 4.0 Hz, 1H), 8.32 (d, ³*J* = 4.0 Hz, 1H), 8.54 (s, 1H), 8.73 (d, ³*J* = 8.80 Hz, 2H), 8.98 (s, 1H). ¹³C NMR (100 MHz, CDCl₃): δ 14.16, 22.63, 26.43, 30.17, 31.35, 57.73, 97.88, 116.03, 116.15, 121.66, 124.32, 125.85, 128.42, 129.23, 129.71, 130.69, 135.77, 138.90, 139.66, 140.23, 145.33, 147.18, 147.34, 148.34, 150.65, 151.41, 166.04. IR (*ν*ₘₐₓ/cm⁻¹, solid): 2922, 2855, 2215, 1714, 1574, 1486, 1433, 1329, 1269, 1193, 811, 753, 695. HRMS (FAB). Calcd for C₃₇H₃₃N₆O₂S ([M + H]⁺): *m/z* 625.2386. Found: *m/z* 625.2387.

2-Cyano-3-[4-[4-[4-(diphenylamino)phenyl]-2-hexyl-2H-[1,2,3]triazolo[4,5-c]pyridin-7-yl]phenyl]acrylic Acid (NPT3). The synthetic procedure was similar to that of **PTN1**. The crude product was purified through flash chromatography using 2% acetic acid in DCM and further recrystallized using a mixture of DCM/acetone to afford **NPT3** as a dark-red solid in 77% yield. ¹H NMR (300 MHz, acetone-*d₆*): δ 0.83−0.89 (m, 3H), 1.28−1.44 (m, 6H), 2.14−2.23 (m, 2H), 4.96 (t, ³*J* = 7.0 Hz, 2H), 7.10−7.23 (m, 8H), 7.35−7.42 (m, 4H), 8.27 (d, ³*J* = 7.4 Hz, 2H), 8.39 (s, 1H), 8.45 (d, ³*J* = 7.5 Hz, 2H), 8.71 (d, ³*J* = 8.6 Hz, 2H), 8.91 (s, 1H). ¹³C NMR (100 MHz, CDCl₃): δ 14.17, 22.64, 26.44, 30.27, 31.35, 57.87, 104.66, 116.46, 121.42, 122.02, 124.54, 125.97, 127.46, 128.99, 129.76, 131.00, 131.83, 138.99, 139.86, 146.73, 146.95, 150.58, 150.98, 153.81, 165.62. IR (*ν*ₘₐₓ/cm⁻¹, solid): 2926, 2857, 2221, 1715, 1587, 1480, 1331, 1268, 1192, 835, 754, 698. HRMS (FAB). Calcd for C₃₉H₃₅N₆O₂ ([M + H]⁺): *m/z* 619.2821. Found: *m/z* 619.2826.

3-[5-[4-[4-[Bis[4-(hexyloxy)phenyl]amino]phenyl]-2-hexyl-2H-[1,2,3]triazolo[4,5-c]pyridin-7-yl]furan-2-yl]-2-cyanoacrylic Acid (NPT4). The synthetic procedure was similar to that of **PTN1**. The crude product was purified through flash chromatography using 2% acetic acid in DCM and further recrystallized using a mixture of DCM/acetone to afford **NPT4** as a dark-brown solid in 87% yield. ¹H NMR (500 MHz, CDCl₃): δ 0.84−0.91 (m, 9H), 1.23−1.51 (m, 18H), 1.71−1.82 (m, 4H), 2.11−2.15 (m, 2H), 3.90−3.95 (m, 4H), 4.72−4.78 (m, 2H), 6.75−6.85 (m, 4H), 6.92−7.05 (m, 2H), 7.06−7.14 (m, 4H), 7.41−7.51 (m, 2H), 8.09 (bs, 1H), 8.50 (bs, 2H), 8.95 (s, 1H). ¹³C NMR (125 MHz, CDCl₃): δ 14.05, 14.13, 22.53, 22.72, 25.87, 26.33, 29.44, 29.99, 31.24, 31.73, 57.46, 68.43, 99.07, 111.37, 115.10, 115.59, 116.37, 118.48, 124.40, 126.43, 127.71, 130.86, 138.75, 139.14, 139.59, 144.21, 148.69, 150.74, 151.60, 154.32, 156.52, 166.10. IR (*ν*ₘₐₓ/cm⁻¹, solid): 2927, 2857, 2221, 1714, 1573, 1504, 1459, 1319, 1237, 1191, 1023, 815, 802, 684. HRMS (FAB). Calcd for C₄₉H₅₇N₆O₅ ([M + H]⁺): *m/z* 809.4390. Found: *m/z* 809.4376.

4-[2-Hexyl-7-(4-hexylthiophen-2-yl)-2H-[1,2,3]triazolo[4,5-c]-pyridin-4-yl]-N,N-diphenylaniline (10). The synthetic procedure was
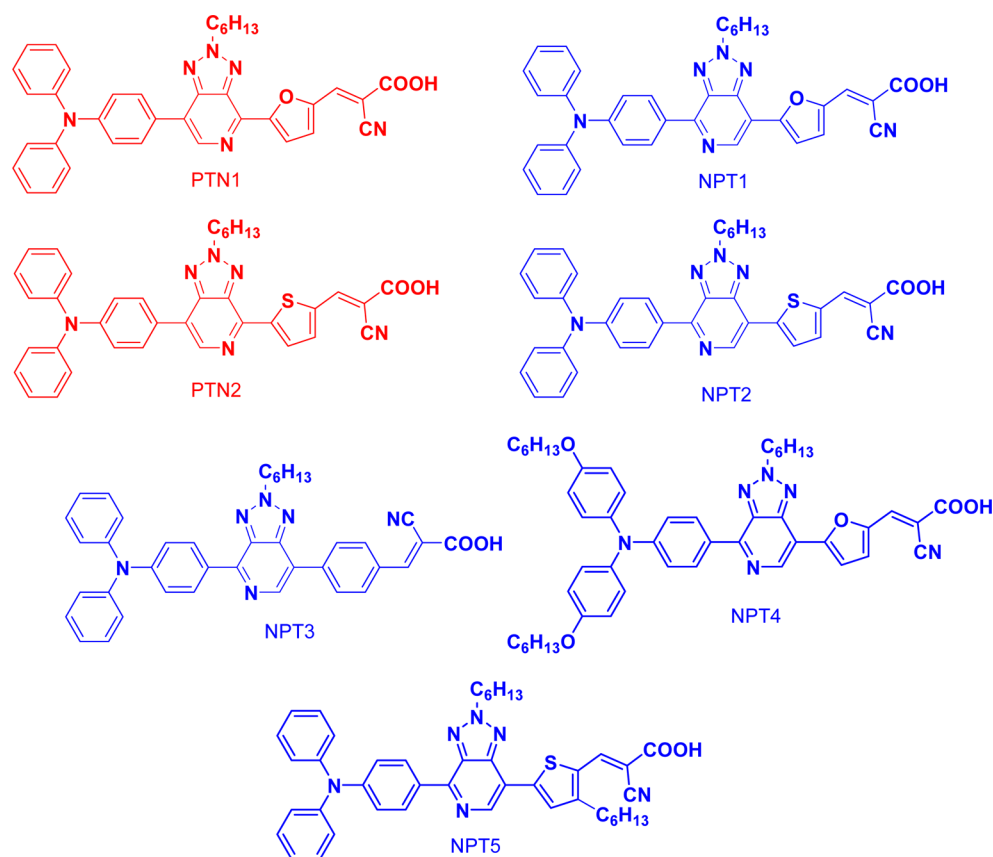
Figure 1. Structures of dyes **PTN***n* (*n* = 1 and 2) and **NPT***n* (*n* = 1−5).

similar to that of **5a**. The crude product was purified by flash chromatography using DCM/hexane (2:1) as the eluent to afford **11** as a yellow solid (83%). ^{1}H NMR (500 MHz, CDCl$_3$): δ 0.87−0.92 (m, 6H), 1.29−1.41 (m, 12H), 1.64−1.73 (m, 2H), 2.14−2.22 (m, 2H), 2.68 (t, ^3J = 7.8 Hz, 2H), 4.82 (t, ^3J = 7.8 Hz, 2H), 6.99 (s, 1H), 7.04−7.09 (m, 2H), 7.15−7.21 (m, 6H), 7.25−7.30 (m, 4H), 7.86−7.87 (m, 1H), 8.54 (d, ^3J = 8.8 Hz, 2H), 8.73 (s, 1H). ^{13}C NMR (125 MHz, CDCl$_3$): δ 14.17, 14.33, 22.65, 22.86, 26.44, 29.25, 30.22, 30.66, 30.81, 31.37, 31.92, 57.41, 117.99, 120.94, 122.44, 123.79, 125.40, 128.93, 129.57, 130.03, 130.58, 137.03, 138.71, 139.79, 144.59, 145.37, 147.47, 149.07, 149.71. MS (FAB): *m/z* 614 ([M + H]$^+$, 100%), 613 ([M]$^+$, 65%).

5-[4-[4-(Diphenylamino)phenyl]-2-hexyl-2H-[1,2,3]triazolo[4,5-c]pyridin-7-yl]-3-hexylthiophene-2-carbaldehyde (11). Compound **10** was dissolved in dry DMF (5 mL) and stirred for 10 min, the mixture was ice-cooled, and then POCl$_3$ (1.2 equiv) was added dropwise under a nitrogen atmosphere. After 5 min, the ice was removed, the temperature was slowly raised to 60 °C, and the solution was stirred for 12 h. After completion, the crude was poured into water, extracted with DCM, dried with MgSO$_4$, filtered, and concentrated. The crude product was purified by flash chromatography using DCM/hexane (4:1) as the eluent to afford **10** as an orange solid (88%). ^{1}H NMR (400 MHz, CDCl$_3$): δ 0.85−0.91 (m, 6H), 1.30−1.42 (m, 12H), 1.70−1.79 (m, 2H), 2.14−2.22 (m, 2H), 3.02 (t, ^3J = 7.8 Hz, 2H), 4.83 (t, ^3J = 7.2 Hz, 2H), 7.05−7.11 (m, 2H), 7.15−7.20 (m, 6H), 7.26−7.32 (m, 4H), 7.89 (s, 1H), 8.56 (d, ^3J = 8.8 Hz, 2H), 8.83 (s, 1H), 10.07 (s, 1H). ^{13}C NMR (125 MHz, CDCl$_3$): δ 14.17, 14.28, 22.65, 22.79, 26.43, 28.85, 29.23, 30.22, 31.35, 31.71, 31.81, 57.57, 116.37, 121.91, 124.11, 125.66, 129.65, 129.82, 130.08, 130.40, 137.18, 139.66, 140.22, 145.37, 146.18, 147.26, 150.31, 151.12, 153.84, 182.22. MS (FAB): *m/z* 642 ([M + H]$^+$, 100%), 613 ([M]$^+$, 70%).

2-Cyano-3-[5-[4-[4-(diphenylamino)phenyl]-2-hexyl-2H-[1,2,3]-triazolo[4,5-c]pyridin-7-yl]-3-hexylthiophen-2-yl]acrylic Acid (NPT5). The synthetic procedure was similar to that of **PTN1**. The crude product was purified through flash chromatography using 2%

acetic acid in DCM and further recrystallized using a mixture of DCM/methanol to afford **NPT5** as a brown solid in 92% yield. ^{1}H NMR (400 MHz, CDCl$_3$): δ 0.88−0.92 (m, 6H), 1.29−1.43 (m, 12H), 1.67−1.77 (m, 2H), 2.13−2.21 (m, 2H), 2.90 (t, ^3J = 7.8 Hz, 2H), 4.79 (t, ^3J = 7.2 Hz, 2H), 7.06−7.14 (m, 4H), 7.15−7.20 (m, 4H), 7.26−7.32 (m, 4H), 7.98 (s, 1H), 8.46 (s, 1H), 8.49 (d, ^3J = 8.8 Hz, 2H), 8.72 (s, 1H). ^{13}C NMR (100 MHz, CDCl$_3$): δ 14.07, 14.18, 22.55, 22.70, 26.35, 29.15, 29.36, 29.97, 31.26, 31.43, 31.69, 57.51, 95.88, 115.93, 116.14, 121.46, 124.18, 125.71, 129.09, 129.59, 129.81, 130.55, 139.39, 140.19, 145.00, 145.07, 146.97, 147.06, 150.40, 151.01, 156.87, 168.15. IR (ν_{max}/cm^{-1}, solid): 2925, 2825, 2214, 1675, 1555, 1518, 1472, 1414, 1318, 1220, 841, 754, 697. HRMS (EI). Calcd for C$_{43}$H$_{44}$N$_6$O$_2$S ([M]$^+$): *m/z* 708.3246. Found: *m/z* 708.3258.

2.3. Device Fabrication. The photoanode used was the TiO$_2$ thin film (12 μm of 20 nm particles as the absorbing layer and 6 μm of 400 nm particles as the scattering layer) coated on an FTO glass substrate with dimensions of 0.4 × 0.4 cm^2.[36] The film thickness was measured by a profilometer (Dektak3, Veeco/Sloan Instruments Inc., Edina, MN). The counter electrode was a platinum-coated FTO substrate that was prepared by sputtering. The TiO$_2$ thin film was dipped into the THF solution containing 3 × 10^{-4} M dye sensitizers for at least 12 h. After rinsing with THF, the photoanode, adhered with a polyester tape of 60 μm thickness and with a square aperture of 0.36 cm^2, was placed on the top of the counter electrode, and they were tightly clipped together to form a cell. Electrolyte was injected into the cell, and the cell was then sealed with the Torr Seal cement (Varian, Lexington, MA). The electrolyte dissolved in acetonitrile was composed of 0.8 M 1-methyl-3-propylimidazolium iodide (PMII), 0.10 M LiI, 0.05 M I$_2$, and 0.5 M 4-*tert*-butylpyridine.

2.4. Quantum Chemistry Computation. The computation was performed with *Q-Chem 4.0* software. Geometry optimization of the molecules was performed using a hybrid B3LYP functional and 6-31G* basis set. For each molecule, a number of possible conformations were examined, and the one with the lowest energy was used. The same functional was also applied for calculation of the

Scheme 1. Synthetic Scheme for All Dyes[a]
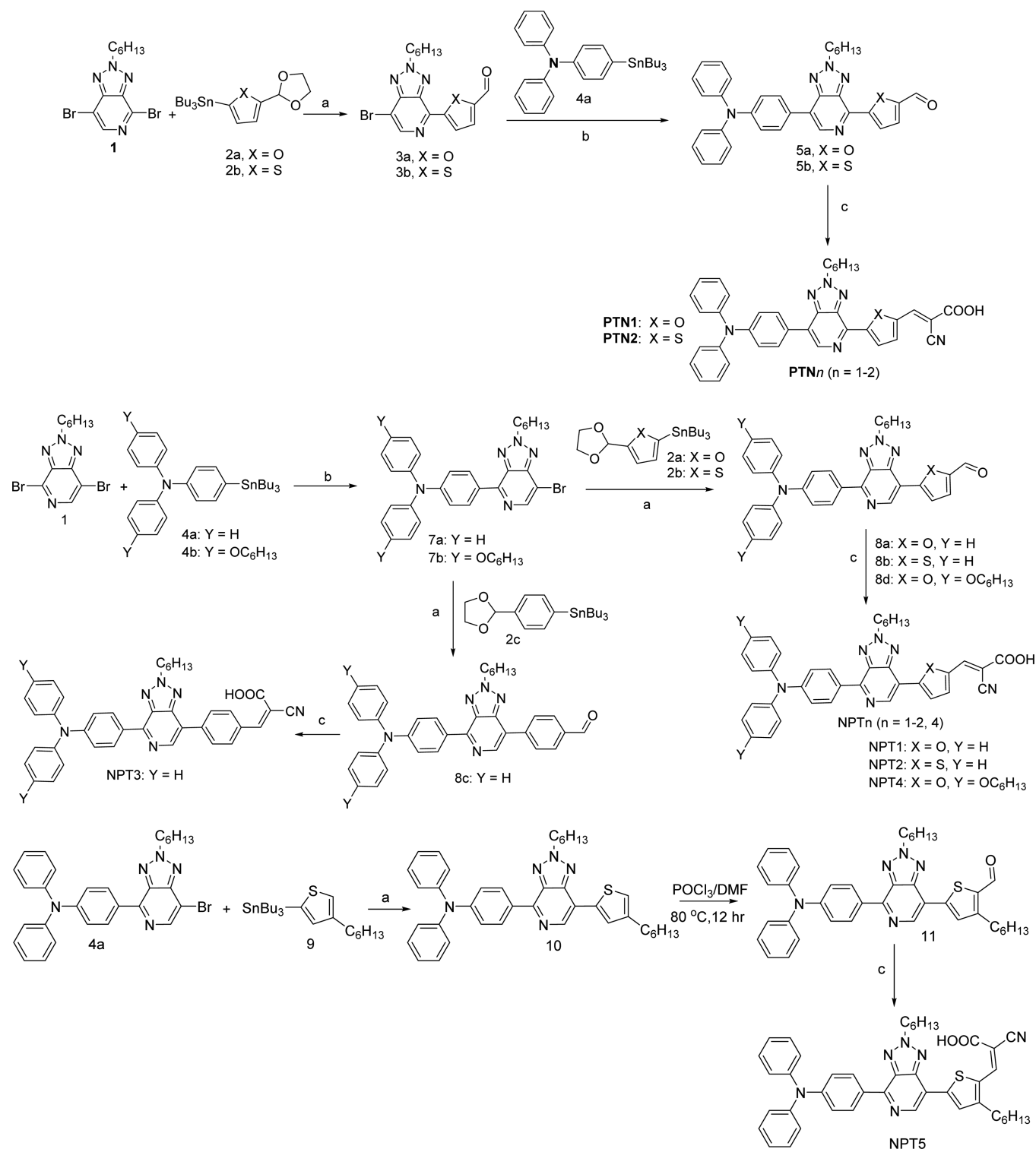
[a]Reaction conditions: (a) (i) PdCl$_2$(PPh$_3$)$_2$, DMF, 80 °C; (ii) AcOH, H$_2$O, 50 °C. (b) PdCl$_2$(PPh$_3$)$_2$, DMF, 80 °C. (c) CNCH$_2$COOH, NH$_4$OAc, AcOH, 100 °C.

excited states using time-dependent density functional theory (TD-DFT). A number of previous works employed TD-DFT to characterize the excited states with charge-transfer character.[37,38] The excitation energies were underestimated in some cases.[37−39] In the present work, we therefore use TD-DFT to visualize the extent of transition moments, as well as their charge-transfer character, and avoid drawing conclusions from the excitation energy.

3. RESULTS AND DISCUSSION

3.1. Synthesis and Characterization. The structures of new metal-free sensitizers are shown in Figure 1, and Scheme 1 illustrates their synthetic protocols. The key steps include Stille coupling and Knoevenagel condensation reactions. The synthesis of a key precursor, 4,7-dibromo-2-hexyl-2H-[1,2,3]-
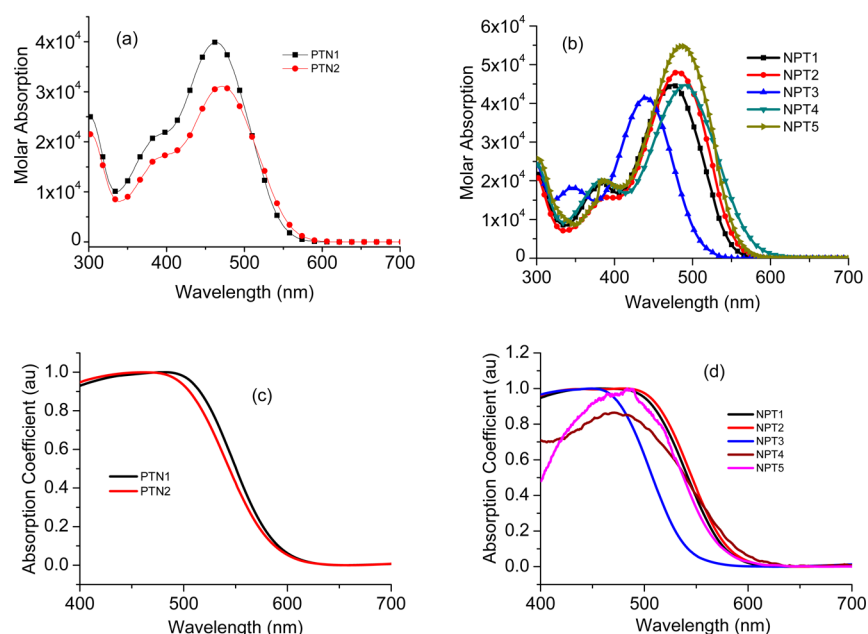
Figure 2. UV−vis absorption spectra of dyes: (a) **PTN**n (n = 1 and 2) and (b) **NPT**n (n = 1−5) in a THF solution (10^{-5} M); (c) **PTN**n (n = 1 and 2) and (d) **NPT**n (n = 1−5) on TiO$_2$.

Table 1. Optical and Electrochemical Data of the Dyes

dye	λ_{abs} ($\varepsilon \times 10^4$ M^{-1} cm^{-1})[a] [nm]	λ_{abs}[b] [nm]	λ_{em}[a] [nm]	E_{ox} (ΔE_p)[c] [mV]	HOMO/LUMO[d] [eV]	E_{0-0}[e] [eV]	E_{0-0}*[f] [V]
PTN1	464 (3.99), 390 (sh, 2.14)	482	571	548 (90)	−5.35/−2.97	2.38	−1.13
PTN2	472 (3.11), 392 (sh, 1.69)	473	583	525 (95)	−5.32/−2.99	2.33	−1.11
NPT1	476 (4.47), 386 (1.95)	476	617	553 (83)	−5.35/−2.98	2.37	−1.12
NPT2	482 (4.80), 390 (1.57)	483	625	562 (81)	−5.36/−3.09	2.27	−1.01
NPT3	440 (4.15), 346 (1.82)	452	553	552 (88)	−5.35/−2.85	2.50	−1.25
NPT4	490 (4.47), 384 (2.01)	488	616	344 (105)	−5.14/−2.91	2.23	−1.19
NPT5	486 (5.48)	486	619	546 (89)	−5.35/−3.09	2.26	−1.01

[a]Recorded in THF (solution). [b]Absorption maxima on a TiO$_2$ film. [c]Recorded in CH$_2$Cl$_2$. Scan rate = 100 mV s^{-1}; electrolyte = [(n-C$_4$H$_9$)$_4$][NPF$_6$]; E_{ox} = $1/2(E_{pa} + E_{pc})$; $\Delta E_p = E_{pa} - E_{pc}$, where E_{pa} and E_{pc} are peak anodic and cathodic potentials, respectively. The oxidation potential reported is adjusted to that of ferrocene (Fc) used as an internal reference. [d]The HOMO and LUMO energies are calculated using the formulas HOMO = 4.8 + ($E_{1/2} - E_{Fc}$) and LUMO = E_{0-0} − HOMO. [e]The optical HOMO/LUMO energy gap, E_{0-0}, was derived from the intersection of the absorption and emission spectra. [f]E_{0-0}*: excited-state oxidation potential vs NHE.

triazolo[4,5-c]pyridine (**1** or **PTBr**$_2$), was described in our previous report.[35] The first Stille coupling of the asymmetric **1** selectively occurred at the position adjacent to the N atom.[40] Consequently, both isomers **PTN**n (n = 1 and 2; N atom facing toward the acceptor) and **NPT**n (n = 1−5; N atom facing away from the acceptor) were successfully obtained by following the pathways described in Scheme 1. The new dyes were well characterized by spectroscopic methods. **PTN**n (n = 1 and 2) were obtained via two successive Stille cross-coupling reactions.[41] Treating **1** with the corresponding [5-(1,3-dioxolan-2-yl)aryl-2-yl]tributylstannane (**2a** and **2b**) afforded aldehydes **3a** and **3b**. The donor was then introduced via a second Stille cross coupling of **3a** and **3b** with N,N-diphenyl-4-(tributylstannyl)aniline (**4**), providing aldehyde derivatives **5a** and **5b**. Finally, Knoevenagel condensation of **5a** and **5b** with cyanoacetic acid afforded the desired products. **NPT**n (n = 1−5) were also obtained via two-step Stille cross-coupling reactions. Treating **1** with the corresponding triarylstannane (**4a** and **4b**) afforded **7a** and **7b**, which then reacted with the corresponding [5-(1,3-dioxolan-2-yl)aryl-2-yl]tributylstannane (**2a**−**2c**) via the second Stille cross-coupling reaction to afford aldehyde intermediates **8a**−**8d**. Subsequent Knoevenagel

condensation of **8a**−**8d** with cyanoacetic acid afforded the desired dyes **NPT**n (n = 1−5). Cross coupling of **4a** with tributyl(4-hexylthiophen-2-yl)stannane afforded **10**, which underwent formylation with POCl$_3$ in DMF to provide **11**. Finally, Knoevenagel condensation of **11** with cyanoacetic acid afforded the desired dye **NPT5**. The yields of the Stille coupling products were from good to excellent. All of the new dyes were characterized through ^{1}H and ^{13}C NMR and mass spectroscopy.

3.2. Photophysical Properties. UV−vis absorption spectra of all dyes in THF are presented in Figure 2a,b, and their corresponding data are summarized in Table 1. The absorption spectra of both series of dyes show two prominent bands in the regions of 350−400 and 400−500 nm. The former can be attributed to the aromatic π−π* transition, and the later broad band is ascribed to the ICT from the triphenylamine donor to the cyanoacetic acid acceptor with some delocalized π−π* transition character.[42] For the isomeric pair of **PTN**n (n = 1 and 2) and **NPT**n (n = 1 and 2), the ICT band of the latter exhibits longer wavelength because of the better planarity (vide infra) of the molecule. The ICT bands of **NPT**n (n = 1 and 2) have larger λ_{max} values than their congener, **NPT3**. This can be
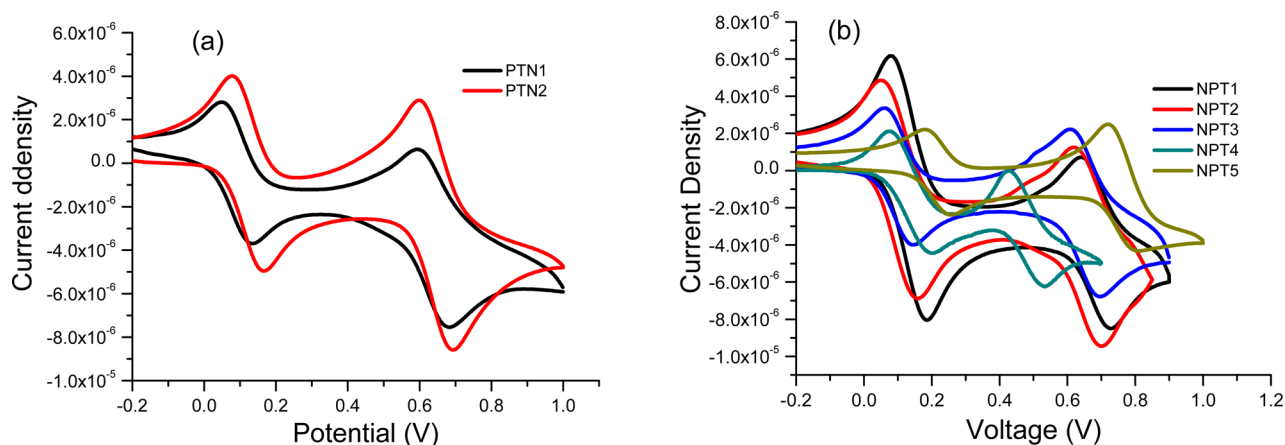
Figure 3. Cyclic voltammograms of (a) **PTN***n* (*n* = 1 and 2) and (b) **NPT3***n* (*n* = 1−5).
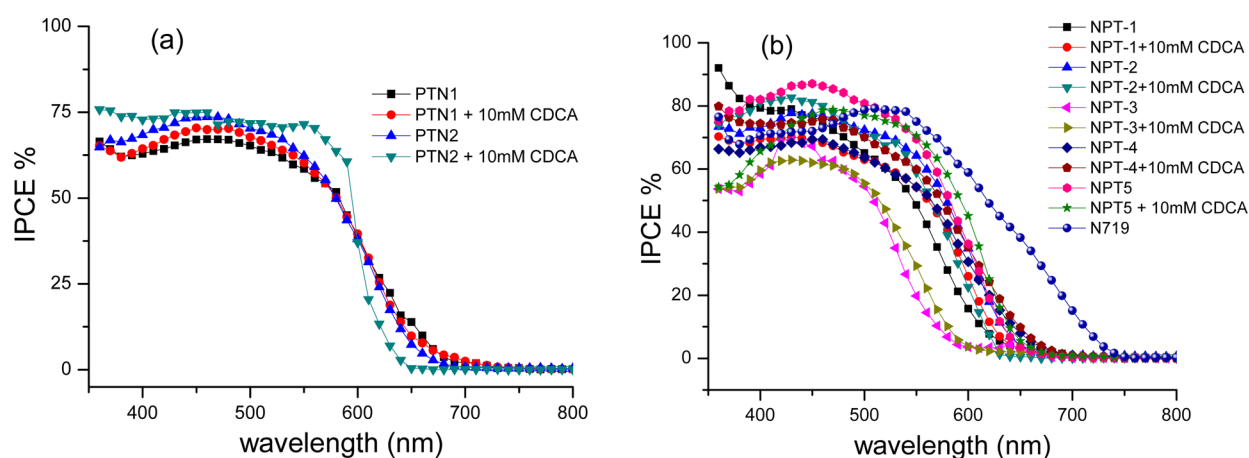

Figure 4. IPCE plots for the DSSCs using (a) **PTN***n* (*n* = 1 and 2) and (b) **NPT***n* (*n* = 1−5) dyes.

attributed to two reasons, leading to less effective charge transfer: (1) the less planar skeleton of **NPT3**; (2) the smaller resonance energy of the thiophenyl and furanyl units in **NPT***n* (*n* = 1 and 2) compared with the phenyl unit in **NPT3**. The longer-wavelength absorption of the thiophene-containing dyes (**PTN2** and **NPT2**) than that of the furan-containing congeners (**PTN1** and **NPT1**) is consistent with the trend normally observed for nonlinear optical chromophores.[43−45] The higher extinction coefficient of **NPT***n* than **PTN***n* is also in accordance with the trend observed in the **PyT** pairs[31] and is most likely due to the better planarity of the conjugated spacer in the former (vide infra). Because the **NPT***n* (*n* = 1 and 2) dyes have a better DSSC performance than the **PTN***n* (*n* = 1 and 2) dyes (vide infra), **PTN4** and **PTN5** were synthesized for possible performance improvement and further study of dye structure versus cell performance. The absorption maxima of **NPT4** is more broadened and red-shifted (∼14 nm) compared to those of **NPT1**, and the onset was shifted from 550 to 600 nm, which can be ascribed to the presence of a stronger donor group, 4,4′-hexyloxyphenylamine. The introduction of a hexyl chain onto the thienyl entity connected to the 2-cyanoacrylic acid anchor was found to be beneficial to suppressing dye aggregation and/or dark current.[46−48] Therefore, **NPT5** was synthesized for such a purpose. Because the alkyl chain does not affect the planarity of the conjugated spacer in the molecule, the spectrum is slightly red-shifted with higher intensity compared with **NPT2**. The ICT bands of the **PT**-

based dyes are blue-shifted by 50−60 nm compared with those of the **PyT**-based dyes,[31] which can be attributed to the higher basicity of the N atom of the **PT** unit. This observation is in conformity with the trend found in **BTA**- and **BT**-based dyes[32−34] and supported by theoretical computations (vide infra).

Parts c and d of Figure 2 show the absorption spectra of the organic dyes adsorbed on a porous TiO$_2$ nanoparticle film (4 μm thickness). Upon adsorption on TiO$_2$, the film spectra of the **NPT***n* and **PTN***n* dyes are broadened and extended to the longer-wavelength region, indicating the presence of both H and J aggregation of the dye molecules.[49,50]

3.3. Electrochemical Properties. The electrochemical properties of **PTN***n* (*n* = 1 and 2) and **NPT***n* (*n* = 1−5) were studied by CV in CH$_2$Cl$_2$ solutions (1.0 mM) with 0.1 M tetra-*n*-butylammonium hexafluorophosphate (TBAPF$_6$) as the supporting electrolyte. The cyclic voltammograms are shown in Figure 3, and the relevant data are compiled in Table 1. All of the dyes exhibit a reversible one-electron redox couple attributed to the oxidation of arylamine. **NPT***n* is oxidized at a slightly higher potential than **PTN***n* because of the shorter distance between the electronegative N atom of **PT** and the arylamine in the former, similar to the trend observed in the **PyT** dyes.[31] The highest occupied molecular orbital (HOMO) energy levels deduced from the redox potentials are in the ranges of 5.32−5.36 and 5.32−5.36 eV for **PTN***n* (*n* = 1 and 2) and **NPT***n* (*n* = 1−5), respectively. This, together with the
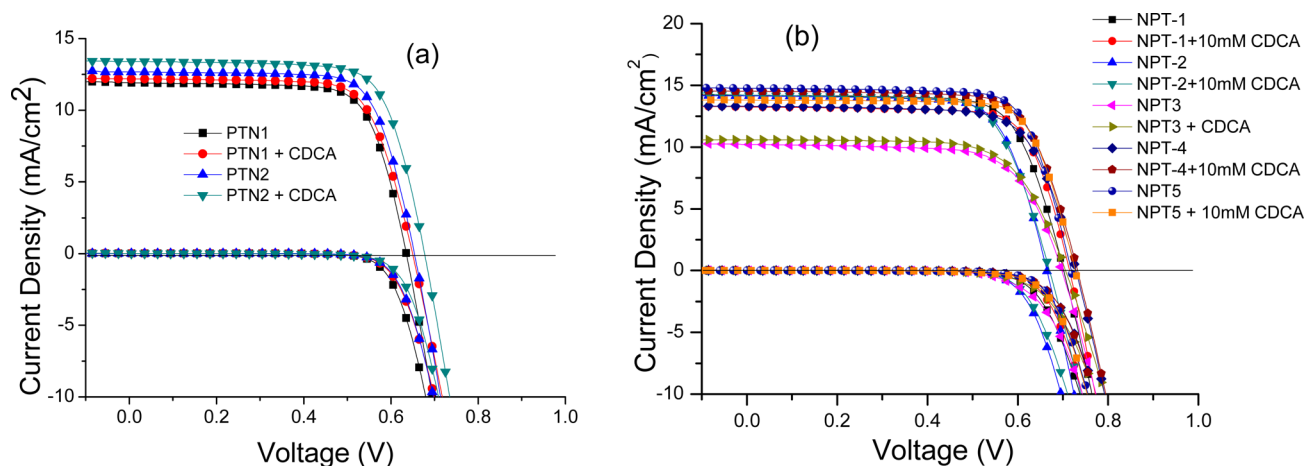
Figure 5. Current density–voltage and dark-current curves of DSSCs based on (a) **PTNn** (n = 1 and 2) and (b) **NPTn** (n = 1−5).

Table 2. Device Performance Parameters of the Dyes with or without CDCA

	V_{OC} [V]	J_{SC} [mA cm^{-2}]	FF	η [%]	dye loading [×10^{-7} mol cm^{-2}]
PTN1	0.636 ± 0.002	11.75 ± 0.19	0.73 ± 0.01	5.45 ± 0.09	3.12
PTN1[a]	0.647 ± 0.006	12.16 ± 0.05	0.72 ± 0.01	5.68 ± 0.07	
PTN2	0.654 ± 0.002	12.80 ± 0.20	0.73 ± 0.01	6.12 ± 0.02	3.14
PTN2[a]	0.677 ± 0.007	13.26 ± 0.18	0.73 ± 0.01	6.57 ± 0.03	
NPT1	0.699 ± 0.006	14.60 ± 0.39	0.71 ± 0.01	7.22 ± 0.03	3.68
NPT1[a]	0.715 ± 0.003	13.59 ± 0.42	0.73 ± 0.01	7.12 ± 0.06	
NPT2	0.665 ± 0.004	13.97 ± 0.27	0.71 ± 0.01	6.64 ± 0.23	3.01
NPT2[a]	0.669 ± 0.001	14.00 ± 0.43	0.71 ± 0.01	6.63 ± 0.11	
NPT3	0.697 ± 0.002	10.24 ± 0.04	0.69 ± 0.01	4.92 ± 0.04	3.54
NPT3[a]	0.706 ± 0.004	10.45 ± 0.25	0.68 ± 0.01	5.02 ± 0.10	
NPT4	0.729 ± 0.002	13.32 ± 0.09	0.71 ± 0.01	6.90 ± 0.04	3.00
NPT4[a]	0.733 ± 0.001	14.37 ± 0.23	0.72 ± 0.01	7.54 ± 0.18	
NPT5	0.720 ± 0.002	14.90 ± 0.14	0.74 ± 0.01	7.92 ± 0.04	2.80
NPT5[a]	0.725 ± 0.001	13.71 ± 0.11	0.74 ± 0.01	7.41 ± 0.11	
N719	0.742 ± 0.003	15.93 ± 0.10	0.70 ± 0.01	8.27 ± 0.08	

[a]With 10 mM CDCA.

HOMO/lowest unoccupied molecular orbital (LUMO) gap (E_{0-0}) obtained from the intersection of absorption/luminescence spectra, was utilized to derive the LUMO energy. The introduction of a stronger donor significantly raises the HOMO level of **NPT4**. The hexyl chain in **NPT5** has only a minimal effect on the oxidation potential of the arylamine, and the HOMO of **NPT5** is comparable with those in **NPT1−NPT3**. The more negative excited-state potential (E_{0-0}*) of the dyes (Table 1), estimated from the first oxidation potential at the ground state and E_{0-0}, than the conduction band edge of TiO$_2$ (−0.5 V vs NHE) will warrant efficient electron injection from the excited dyes into the TiO$_2$ electrode. Regeneration of the dyes is also thermodynamically feasible because of the more positive oxidation potential of the dyes compared with that of the I$^-$/I$_3^-$ redox potential (∼0.35 V vs NHE).

3.4. Photovoltaic Properties. DSSCs with an effective area of 0.16 cm^2 and an electrolyte composed of 0.8 M PMII, 0.10 M LiI, 0.05 M I$_2$, and 0.5 M TBP in an acetonitrile solution were fabricated to explore the potentials of new dyes as sensitizers. The incident photon-to-current conversion efficiency (IPCE) plots of the cells, and the typical photocurrent–voltage (J−V) curves of the devices under AM 1.5G (100 mW cm^{-2}) illumination and in the dark are shown in Figures 4 and 5, respectively. The corresponding open-circuit voltage (V_{OC}), short-circuit photocurrent density (J_{SC}), fill factor (FF), and

PCE values are summarized in Table 2. The dye loading measured (Table 2) is similar for different cells and is considered not to be the dominating factor for the cell performance. J_{SC}, V_{OC}, and FF of the devices are in the ranges of 7.88−14.90 mA cm^{-2}, 0.63−0.73 V, and 0.68−0.74, respectively, corresponding to an overall conversion efficiency (η) of 3.59−7.92%. The maximum efficiencies of 7.92% (∼96% of a N719-based standard cell fabricated and measured under similar conditions) and 7.22% were obtained with **NPT5** and **NPT1**, respectively. The higher efficiency of **NPT1** (or **NPT2**) than **PTN1** (or **PTN2**) can be attributed mainly to the better light harvesting of the former, which is also reflected from the higher current density of the former (vide supra). Improved V_{OC} values due to the slightly better dark current suppression (see EIS studies, vide infra) may also contribute to the better cell performance of the **NPT** dyes. Possibly the larger twist angle (**PTN1**, 26.9°; **PTN2**; 26.0°; **NPT1**, 0.9°; **NPT2**, −0.4°) between the donor and PT unit for the **PTN** series can more effectively block the oxidized electrolytes from approaching the TiO$_2$ surface. Significantly lower cell efficiency of **NPT3** compared with **NPT1** and **NPT2** can be largely ascribed to its lower current density because of less efficient light harvesting. Although **NPT4** exhibits better light harvesting than **NPT1** because of its stronger electron-donating arylamine, it has a lower current density than the latter. Possibly the higher
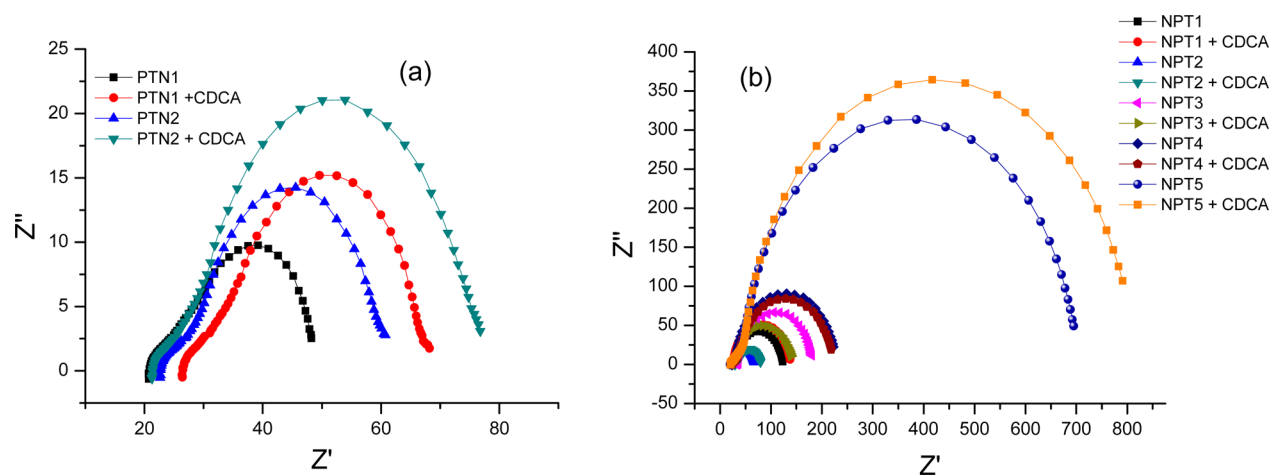
Figure 6. EIS spectra (Nyquist plots) of DSSC for (a) **PTN***n* (*n* = 1 and 2) and (b) **NPT***n* (*n* = 1−5) dyes measured in the dark under −0.65 V bias.

HOMO level of **NPT4** results in less efficient dye regeneration and attenuates electron injection. It is interesting that two hexyloxy substituents at the amine donor of **NPT4** render the dye able to more effectively suppress the dark current compared with **NPT1**−**NPT3** (vide infra), leading to a higher V_{OC}.[51] The most striking accomplishment in this study is the high efficiency of **NPT5**, which reaches ∼96% of the standard DSSC fabricated from N719 (8.27%). Such an outcome can be rationalized by two main reasons: (1) **NPT5** has broader and longer wavelength among the dyes; (2) **NPT5** has the most effective dark-current suppression (vide infra). Evidently, the incorporation of the hexyl substituent at the thiophene ring is beneficial to dark-current suppression. We also observed similar behavior of the hexyl substituent in our previous reports on phenothiazine-based sensitizers possessing two anchors.[52,53]

Because the spectra of the dyes on TiO$_2$ indicated that there was slight dye aggregation, CDCA was also added for alleviation of dye aggregation. The addition of CDCA slightly improves both the J_{SC} and V_{OC} values for **PTN1** and **PTN2**, indicating that CDCA helps with alleviation of the dyes. For **NPT** dyes, the cell performance remains about the same except for **NPT4** and **NPT5**. The cell efficiency drops by ∼0.5% for **NPT5** after the addition of CDCA. This suggests that antiaggregation of dye molecules does not compensate for the loss of the dye loading amount. In contrast, the cell efficiency of **NPT4** increases by ∼0.6% after the addition of CDCA, mainly because of the increment (by ∼1 mA cm^{-2}) of the J_{SC} value. On the basis of a similar recombination resistance from EIS studies (vide infra) for the DSSCs with and without CDCA, the outcome may be attributed to the alleviation of dye aggregation by added CDCA.

EIS can provide important information on the interfacial charge recombination and electron-transport process in DSSCs. Figure 6 shows the Nyquist plots under a forward bias of −0.65 V in the dark. The second semicircle is related to the resistance of the recombination (R_{rec}) between the electrons on the TiO$_2$ surface and the oxidized electrolyte, which can be deduced from fitting curves from the range of intermediate frequency using Z-view software.[54−57] A smaller R_{rec} value indicates a faster charge recombination, which will decrease the V_{OC} value. The much smaller R_{rec} values for **PTN***n* (*n* = 1 and 2) than their isomeric congeners **NPT***n* (*n* = 1 and 2) implies a faster charge recombination in **PTN***n*, which is consistent with the lower V_{OC} values of **PTN***n*-based cells. The R_{rec} values for DSSCs

based on **NPT1**−**NPT5** sensitizers decrease in the order of **NPT5** > **NPT4** > **NPT3** > **NPT1** > **NPT2**. The trend observed here is nearly in parallel with the trend of the V_{OC} values, **NPT4** ≈ **NPT5** > **NPT1** ≈ **NPT3** > **NPT2**. **NPT4**-sensitized (0.729 V) and **NPT5**-sensitized (0.720 V) DSSCs show the highest V_{OC} values, confirming that the hexylthiophene unit in **NPT5** and the hexyloxy substituents at the amine donor of **NPT4** indeed help with retarding the charge recombination between the TiO$_2$ film and the electrolyte, i.e., dark current.

3.5. Theoretical Approach. The charge excitation behavior for the dyes is further examined via DFT calculations. Selected frontier orbitals of the dyes are shown in Figure 7 and Supporting Information (Figure S3). The HOMO in these compounds is mainly distributed from arylamine extending to the conjugated spacer, and the LUMO is largely distributed from 2-cyanoacrylic acid extending to the spacer. The strong ICT behavior of both series of dyes is evident from the corresponding $S_0 \rightarrow S_1$ excitation energy (λ_{cal}: 2.03−2.13 eV for **PTN***n* and 1.89−2.18 eV for **NPT***n*) and oscillator strength (f: 0.58−0.63 for **PTN***n* and 0.61−0.93 for **NPT***n*). The dihedral angles between successive units of the molecules are shown in Figure S2. The more planar structure of **NPT***n* (*n* = 1 and 2) than that of **PTN***n* (*n* = 1 and 2) should be the cause of the higher absorption intensity of the former. The presence of the hexyl substituent in **NPT5** does not appear to affect the planarity of the dye molecule.

Differences in the Mulliken charges in the excited and ground states were calculated and grouped into several segments in the molecules to estimate the extent of charge separation upon excitation. The Mulliken charge variation during electronic transition calculated from the TD-DFT results[58] is shown in Table S1, and the charge variation for the S_1 and S_2 states is shown in Figure S1. The molecules are divided into four segments: the donor group (**TPA**), **PT**, the heteroaromatic ring (spacer), and the acceptor/anchor 2-cyanoacrylic acid (**An**). Compared with **PyT** congeners,[31] in which the **PyT** entity is the second electron acceptor, the negative charge at the second acceptor is smaller for the **PT** dyes. Our preliminary results indicate that the **PT** dyes have a cell efficiency of nearly 1 order better compared with the **PyT** dyes. In order to test the possible correlation of the Mulliken charge with the cell performance, we carry out Mulliken charge analysis (Figure S5) on a series of congeners with similar structure except for the second acceptor (Figure 8): **NPT2**
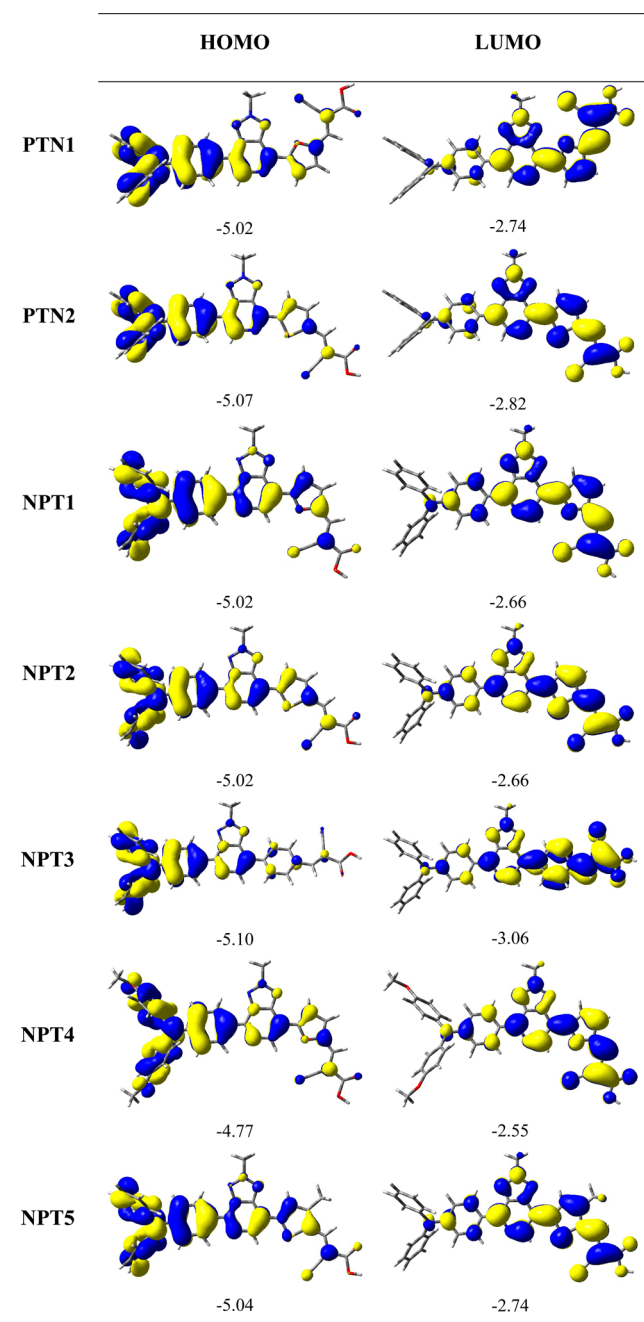
Figure 7. Selected frontier orbitals of the dyes.

Figure 8. Mulliken charge analysis on a series of congeners with similar structure except for the second acceptor, **PT**, **PyT**, **BT**, and **BTz**.

4. CONCLUSIONS

In summary, we have successfully developed a new series of sensitizers incorporating an electron-deficient 2*H*-[1,2,3]-triazolo[4,5-*c*]pyridine as the second acceptor in the conjugated spacer of metal-free dipolar sensitizers for DSSCs. By appropriate tuning of the conjugated spacer, the best conversion efficiency can reach 7.92%, which is ~96% of the ruthenium dye N719-based reference cell measured under the same conditions. Comparisons of the absorption spectra, Mulliken charges, and cell efficiencies were made on **NPT2** (2*H*-[1,2,3]triazolo[4,5-*c*]pyridine as the second acceptor) and three structurally similar D−A−π−A-type congeners with different second acceptors, **BT**, **BTA**, and **PyT**. A more electron-deficient second acceptor leads to a more negative Mulliken charge, and the corresponding sensitizer has a more red-shifted ICT band. However, a highly negative Mulliken charge does not necessarily lead to a better cell performance because of inefficient electron injection, as is evidenced by the lowest cell performance of the **PyT**-based dye. The **BTA**-based dye has the smallest negative Mulliken charge; still, its cell efficiency is lower than that of the **NPT2** dye because of insufficient light harvesting. The highest cell efficiency of **NPT2** among all can be attributed to a good compromise between light harvesting and charge trapping (electron injection). The change in the Mulliken charges of the second acceptor of the dyes for the $S_0 \rightarrow S_1$ transition seems to be a good semiempirical index for electron injection and therefore the cell performance.

ASSOCIATED CONTENT

S **Supporting Information**

The Supporting Information is available free of charge on the ACS Publications website at DOI: 10.1021/acsami.5b07205.

> Complete experimental details and spectroscopy data, ^{1}H and ^{13}C NMR of all new dyes, and details of the theoretical calculation (PDF)

AUTHOR INFORMATION

Corresponding Author

*E-mail: jtlin@gate.sinica.edu.tw.

Author Contributions

†The first two authors contributed equally to this research.

Notes

The authors declare no competing financial interest.

(second acceptor = **PT**), **SC-NPyT2** (second acceptor = **PyT**), **S1** (second acceptor = **BT**), and **BTA-III** (second acceptor = **BTA**). The dyes **NPT2**, **SC-NPyT2**,[31] **BTA-III**,[33] and **S1**[59] have absorption maxima at 482, 546, 454, and 491 nm and cell efficiencies of 6.64%, 1.16%, 5.47%, and 5.01%, respectively. **SC-NPyT2** has the most negative charge and the lowest cell efficiency in spite of its longest absorption wavelength. Although **BTA-III** has the least negative charge among all, it has the shortest absorption wavelength, and its cell efficiency is lower than that of **NPT2**. Therefore, a compromise between red shifting of the absorption spectrum and charge trapping is important when the second acceptor in the D−A−π−A system is chosen, and the Muliken charge at the second acceptor seems to be a useful semiempirical index for the cell efficiency of structurally similar sensitizers.
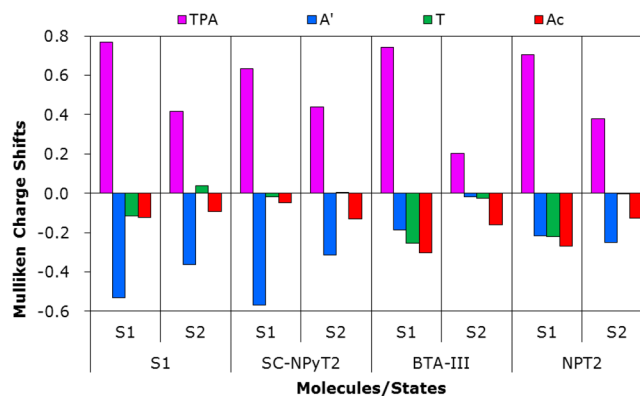
■ REFERENCES

(1) Parisi, M. L.; Maranghi, S.; Basosi, R. The Evolution of the Dye Sensitized Solar Cells from Grätzel Prototype to up-Scaled Solar Applications: A Life Cycle Assessment Approach. *Renewable Sustainable Energy Rev.* **2014**, *39*, 124−138.

(2) Hagfeldt, A.; Boschloo, G.; Sun, L.; Kloo, L.; Pettersson, H. Dye-Sensitized Solar Cells. *Chem. Rev.* **2010**, *110*, 6595−6663.

(3) Ganesh, I. Solar Fuels vis-à-vis Electricity Generation from Sunlight: The Current State-of-the-Art (a review). *Renewable Sustainable Energy Rev.* **2015**, *44*, 904−932.

(4) O'Regan, B.; Grätzel, M. A Low-Cost, High-Efficiency Solar Cell Based on Dye-Sensitized Colloidal TiO_2 Films. *Nature* **1991**, *353*, 737−740.

(5) Mathew, S.; Yella, A.; Gao, P.; Humphry-Baker, R.; Curchod, B. F. E.; Ashari-Astani, N.; Tavernelli, I.; Rothlisberger, U.; Nazeeruddin, M. K.; Grätzel, M. Dye-Sensitized Solar Cells with 13% Efficiency Achieved Through the Molecular Engineering of Porphyrin Sensitizers. *Nat. Chem.* **2014**, *6*, 242−247.

(6) Yao, Z.; Zhang, M.; Wu, H.; Yang, L.; Li, R.; Wang, P. Donor/Acceptor Indenoperylene Dye for Highly Efficient Organic Dye-Sensitized Solar Cells. *J. Am. Chem. Soc.* **2015**, *137*, 3799−3802.

(7) Ning, Z.; Fu, Y.; Tian, H. Improvement of Dye-Sensitized Solar Cells: What we Know and What we Need to Know. *Energy Environ. Sci.* **2010**, *3*, 1170−1181.

(8) Zhang, M.; Wang, Y.; Xu, M.; Ma, W.; Li, R.; Wang, P. Design of High-Efficiency Organic Dyes for Titania Solar Cells Based on the Chromophoric Core of Cyclopentadithiophene-Benzothiadiazole. *Energy Environ. Sci.* **2013**, *6*, 2944−2949.

(9) Huang, Z. S.; Feng, H. L.; Zang, X. F.; Iqbal, Z.; Zeng, H. P.; Kuang, D. B.; Wang, L. Y.; Meier, H.; Cao, D. R. Dithienopyrrolo-benzothiadiazole-Based Organic Dyes for Efficient Dye-Sensitized Solar Cells. *J. Mater. Chem. A* **2014**, *2*, 15365−15376.

(10) Tang, J.; Wu, W. J.; Hua, J. L.; Li, J.; Li, X.; Tian, H. Starburst Triphenylamine-Based Cyanine Dye for Efficient Quasi-Solid-State Dye-Sensitized Solar Cells. *Energy Environ. Sci.* **2009**, *2*, 982−990.

(11) Chen, Y. C.; Chen, Y. H.; Chou, H. H.; Chaurasia, S.; Wen, Y. S.; Lin, J. T.; Yao, C. F. Naphthyl and Thienyl Units as Bridges for Metal-Free Dye-Sensitized Solar Cells. *Chem. - Asian J.* **2012**, *7*, 1074−1084.

(12) Olivier, C.; Sauvage, F.; Ducasse, L.; Castet, F.; Grätzel, M.; Toupance, T. Fine-Tuning of Triarylamine-Based Photosensitizers for Dye-Sensitized Solar Cells. *ChemSusChem* **2011**, *4*, 731−736.

(13) Hua, Y.; Chang, S.; Huang, D. D.; Zhou, X.; Zhu, X. J.; Zhao, J. Z.; Chen, T.; Wong, W. Y.; Wong, W. K. Significant Improvement of Dye-Sensitized Solar Cell Performance Using Simple Phenothiazine-Based Dyes. *Chem. Mater.* **2013**, *25*, 2146−2153.

(14) Siva Kumar, G.; Srinivas, K.; Shanigaram, B.; Bharath, D.; Singh, S. P.; Bhanuprakash, K.; Rao, V. J.; Islam, A.; Han, L. Metal-free organic dyes containing thiadiazole unit for dye-sensitized solar cells: a combined experimental and theoretical study. *RSC Adv.* **2014**, *4*, 13172−13181.

(15) Singh, S. P.; Roy, M. S.; Thomas, K. R. J.; Balaiah, S.; Bhanuprakash, K.; Sharma, G. D. New Triphenylamine-Based Organic Dyes with Different Numbers of Anchoring Groups for Dye-Sensitized Solar Cells. *J. Phys. Chem. C* **2012**, *116*, 5941−5950.

(16) Mishra, A.; Fischer, M. K. R.; Bauerle, P. Metal-Free Organic Dyes for Dye-Sensitized Solar Cells: From Structure: Property Relationships to Design Rules. *Angew. Chem., Int. Ed.* **2009**, *48*, 2474−2499.

(17) Kim, S. H.; Kim, H. W.; Sakong, C.; Namgoong, J.; Park, S. W.; Ko, M. J.; Lee, C. H.; Lee, W. I.; Kim, J. P. Effect of Five-Membered Heteroaromatic Linkers to the Performance of Phenothiazine-Based Dye-Sensitized Solar Cells. *Org. Lett.* **2011**, *13*, 5784−5787.

(18) Chen, J.-H.; Tsai, C.-H.; Wang, S.-A.; Lin, Y.-Y.; Huang, T.-W.; Chiu, S.-F.; Wu, C.-C.; Wong, K.-T. Organic Dyes Containing a Coplanar Indacenodithiophene Bridge for High-Performance Dye-Sensitized Solar Cells. *J. Org. Chem.* **2011**, *76*, 8977−8985.

(19) Hong, Y. P.; Liao, J.-Y.; Cao, D. R.; Zang, X. F.; Kuang, D.-B.; Wang, L. Y.; Meier, H.; Su, C.-Y. Organic Dye Bearing Asymmetric Double Donor-π-Acceptor Chains for Dye-Sensitized Solar Cells. *J. Org. Chem.* **2011**, *76*, 8015−8021.

(20) Haid, S.; Marszalek, M.; Mishra, A.; Wielopolski, M.; Teuscher, J.; Moser, J.-E.; Humphry-Baker, R.; Zakeeruddin, S. M.; Grätzel, M.; Bäuerle, P. Significant Improvement of Dye-Sensitized Solar Cell Performance by Small Structural Modification in π-Conjugated Donor−Acceptor Dyes. *Adv. Funct. Mater.* **2012**, *22*, 1291−1302.

(21) Chaurasia, S.; Chen, Y.-C.; Chou, H.-H.; Wen, Y.-S.; Lin, J. T. Coplanar Indenofluorene-Based Organic Dyes for Dye-Sensitized solar cells. *Tetrahedron* **2012**, *68*, 7755−7762.

(22) Paramasivam, M.; Chitumalla, R. K.; Singh, S. P.; Islam, A.; Han, L.; Jayathirtha Rao, V.; Bhanuprakash, K. Tuning the Photovoltaic Performance of Benzocarbazole-Based Sensitizers for Dye-Sensitized Solar Cells: A Joint Experimental and Theoretical Study of the Influence of π−Spacers. *J. Phys. Chem. C* **2015**, *119*, 17053−17064.

(23) Gupta, K. S. V.; Suresh, T.; Singh, S. P.; Islam, A.; Han, L.; Chandrasekharam, M. Carbazole based A-π-D-π-A dyes with double electron acceptor for dye-sensitized solar cell. *Org. Electron.* **2014**, *15*, 266−275.

(24) Gupta, K. S. V.; Singh, S. P.; Islam, A.; Han, L.; Chandrasekharam, M. Simple Fluorene Based Triarylamine Metal-Free Organic Sensitizers. *Electrochim. Acta* **2015**, *174*, 581−587.

(25) Wan, Z.; Jia, C.; Duan, Y.; Zhou, L.; Lin, Y.; Shi, Y. Phenothiazine−triphenylamine based organic dyes containing various conjugated linkers for efficient dye-sensitized solar cells. *J. Mater. Chem.* **2012**, *22*, 25140−25147.

(26) Velusamy, M.; Thomas, K. R. J.; Lin, J. T.; Hsu, Y.-C.; Ho, K.-C. Organic Dyes Incorporating Low-Band-Gap Chromophores for Dye-Sensitized Solar Cells. *Org. Lett.* **2005**, *7*, 1899−1902.

(27) Wu, Y.; Zhu, W. Organic Sensitizers from D−π−A to D−A−π−A: Effect of the Internal Electron-Withdrawing Units on Molecular Absorption, Energy Levels and Photovoltaic Performances. *Chem. Soc. Rev.* **2013**, *42*, 2039−2058.

(28) Qu, S.; Qin, C.; Islam, A.; Wu, Y.; Zhu, W.; Hua, J.; Tian, H.; Han, L. A novel D−A-π-A Organic Sensitizer Containing a Diketopyrrolopyrrole Unit with a Branched Alkyl Chain for Highly Efficient and Stable Dye-Sensitized Solar Cells. *Chem. Commun.* **2012**, *48*, 6972−6974.

(29) Pei, K.; Wu, Y.; Islam, A.; Zhang, Q.; Han, L.; Tian, H.; Zhu, W. Constructing High-Efficiency D−A−π−A Featured Solar Cell Sensitizers: a Promising Building Block of 2,3-Diphenylquinoxaline for Antiaggregation and Photostability. *ACS Appl. Mater. Interfaces* **2013**, *5*, 4986−4995.

(30) Wu, Y.; Zhu, W.-H.; Zakeeruddin, S. M.; Grätzel, M. Insight into D−A−π−A Structured Sensitizers: A Promising Route to Highly Efficient and Stable Dye-Sensitized Solar Cells. *ACS Appl. Mater. Interfaces* **2015**, *7*, 9307−9318.

(31) Chaurasia, S.; Hsu, C.-Y.; Chou, H.-H.; Lin, J. T. Synthesis, Optical and Electrochemical Properties of Pyridal[2,1,3]thiadiazole Based Organic Dyes for Dye Sensitized Solar Cells. *Org. Electron.* **2014**, *15*, 378−390.

(32) Yen, Y. S.; Lee, C. T.; Hsu, C. Y.; Chou, H.-H.; Chen, Y. C.; Lin, J. T. Benzotriazole-Containing D−π−A Conjugated Organic Dyes for Dye-Sensitized Solar Cells. *Chem. - Asian J.* **2013**, *8*, 809−816.

(33) Mao, J.; Guo, F.; Ying, W.; Wu, W.; Li, J.; Hua, J. Benzotriazole-Bridged Sensitizers Containing a Furan Moiety for Dye-Sensitized Solar Cells with High Open-Circuit Voltage Performance. *Chem. - Asian J.* **2012**, *7*, 982−991.

(34) Cui, Y.; Wu, Y.; Lu, X.; Zhang, X.; Zhou, G.; Miapeh, F. B.; Zhu, W.; Wang, Z.-S. Incorporating Benzotriazole Moiety to Construct D−A−π−A Organic Sensitizers for Solar Cells: Significant Enhancement of Open-Circuit Photovoltage with Long Alkyl Group. *Chem. Mater.* **2011**, *23*, 4394−4401.

(35) Chaurasia, S.; Hung, W.-I; Chou, H.-H.; Lin, J. T. Incorporating a New 2*H*-[1,2,3]Triazolo[4,5-*c*]pyridine Moiety To Construct D−A−π−A Organic Sensitizers for High Performance Solar Cells. *Org. Lett.* **2014**, *16*, 3052−3055.

(36) Yen, Y. S.; Chen, Y. C.; Hsu, Y. C.; Chou, H.-H.; Lin, J. T.; Yin, D. J. Heteroleptic Ruthenium Sensitizers That Contain an Ancillary Bipyridine Ligand Tethered with Hydrocarbon Chains for Efficient Dye-Sensitized Solar Cells. *Chem. - Eur. J.* **2011**, *17*, 6781−6788.

(37) Vaswani, H. M.; Hsu, C.-P.; Head-Gordon, M.; Fleming, G. R. Quantum Chemical Evidence for an Intramolecular Charge-Transfer State in the Carotenoid Peridinin of Peridinin−Chlorophyll−Protein. *J. Phys. Chem. B* **2003**, *107*, 7940−7946.

(38) Kurashige, Y.; Nakajima, T.; Kurashige, S.; Hirao, K.; Nishikitani, Y. Theoretical Investigation of the Excited States of Coumarin Dyes for Dye-Sensitized Solar Cells. *J. Phys. Chem. A* **2007**, *111*, 5544−5548.

(39) Dreuw, A.; Head-Gordon, M. Failure of Time-Dependent Density Functional Theory for Long-Range Charge-Transfer Excited States: The Zincbacteriochlorin−Bacteriochlorin and Bacteriochlorophyll−Spheroidene Complexes. *J. Am. Chem. Soc.* **2004**, *126*, 4007−4016.

(40) Handy, S. T.; Wilson, T.; Muth, A. Disubstituted Pyridines: The Double-Coupling Approach. *J. Org. Chem.* **2007**, *72*, 8496−8500.

(41) Tunney, S. E.; Stille, J. K. Palladium-catalyzed coupling of aryl halides with (trimethylstannyl)diphenylphosphine and (trimethylsilyl)diphenylphosphine. *J. Org. Chem.* **1987**, *52*, 748−753.

(42) Yang, H. Y.; Yen, Y. S.; Hsu, Y. C.; Chou, H. H.; Lin, J. T. Organic Dyes Incorporating the Dithieno[3,2-*b*:2′,3′-*d*]thiophene Moiety for Efficient Dye-Sensitized Solar Cells. *Org. Lett.* **2010**, *12*, 16−19.

(43) Jen, A. K.-Y.; Rao, V. P.; Wong, K. Y.; Drost, K. J. Functionalized Thiophenes: Second-Order Nonlinear Optical Materials. *J. Chem. Soc., Chem. Commun.* **1993**, 90−92.

(44) Rao, V. P.; Cai, Y. M.; Jen, A. K.-Y. Ketene Dithioacetal as a π-Electron Donor in Second-Order Nonlinear Optical Chromophores. *J. Chem. Soc., Chem. Commun.* **1994**, 1689−1690.

(45) Jen, A. K.-Y.; Cai, Y.; Bedworth, P. V.; Marder, S. R. Synthesis and Characterization of Highly Efficient and Thermally Stable Diphenylamino-Substituted Thiophene Stilbene Chromophores for Nonlinear Optical Applications. *Adv. Mater.* **1997**, *9*, 132−135.

(46) Kroeze, J. E.; Hirata, N.; Koops, S.; Nazeeruddin, Md. K.; Schmidt-Mende, L.; Gratzel, M.; Durrant, J. R. Alkyl Chain Barriers for Kinetic Optimization in Dye-Sensitized Solar Cells. *J. Am. Chem. Soc.* **2006**, *128*, 16376−16383.

(47) Wang, Z.-S.; Koumura, N.; Cui, Y.; Takahashi, M.; Sekiguchi, H.; Mori, A.; Kubo, T.; Furube, A.; Hara, K. Hexylthiophene-Functionalized Carbazole Dyes for Efficient Molecular Photovoltaics: Tuning of Solar-Cell Performance by Structural Modification. *Chem. Mater.* **2008**, *20*, 3993−4003.

(48) Wu, Y.; Zhang, X.; Li, W.; Wang, Z.-S.; Tian, H.; Zhu, W. Hexylthiophene-Featured D−A−π−A Structural Indoline Chromophores for Coadsorbent-Free and Panchromatic Dye-Sensitized Solar Cells. *Adv. Energy Mater.* **2012**, *2*, 149−156.

(49) Thomas, K. R. J.; Hsu, Y.-C.; Lin, J. T.; Lee, K.-M.; Ho, K.-C.; Lai, C.-H.; Cheng, Y.-M.; Chou, P.-T. 2,3-Disubstituted Thiophene-Based Organic Dyes for Solar Cells. *Chem. Mater.* **2008**, *20*, 1830−1840.

(50) He, J.; Wu, W.; Hua, J.; Jiang, Y.; Qu, S.; Li, J.; Long, Y.; Tian, H. Bithiazole-Bridged Dyes for Dye-Sensitized Solar Cells with High Open Circuit Voltage Performance. *J. Mater. Chem.* **2011**, *21*, 6054−6062.

(51) Li, H.; Yang, Y.; Hou, Y.; Tang, R.; Duan, T.; Chen, J.; Wang, H.; Han, H.; Peng, T.; Chen, X.; Li, Q.; Li, Z. *ACS Sustainable Chem. Eng.* **2014**, *2*, 1776−1784.

(52) Hung, W.-I; Liao, Y.-Y.; Hsu, C.-Y.; Chou, H.-H.; Lee, T.-H.; Kao, W.-S.; Lin, J. T. High-Performance Dye-Sensitized Solar Cells Based on Phenothiazine Dyes Containing Double Anchors and Thiophene Spacers. *Chem. - Asian J.* **2014**, *9*, 357−366.

(53) Hung, W.-I; Liao, Y.-Y.; Lee, T.-H.; Ting, Y.-C.; Ni, J.-S.; Kao, W.-S.; Lin, J. T.; Wei, T.-C.; Yen, Y.-S. Eugenic Metal-Free Sensitizers with Double Anchors for High Performance Dye-Sensitized Solar Cells. *Chem. Commun.* **2015**, *51*, 2152−2155.

(54) Han, L. Y.; Koide, N.; Chiba, Y.; Islam, A.; Komiya, R.; Fuke, N.; Fukui, A.; Yamanaka, R. Improvement of Efficiency of Dye-Sensitized Solar Cells by Reduction of Internal Resistance. *Appl. Phys. Lett.* **2005**, *86*, 213501.

(55) Wang, Q.; Moser, J. E.; Grätzel, M. Electrochemical Impedance Spectroscopic Analysis of Dye-Sensitized Solar Cells. *J. Phys. Chem. B* **2005**, *109*, 14945−14953.

(56) Kern, R.; Sastrawan, R.; Ferber, J.; Stangl, R.; Luther, J. Modeling and Interpretation of Electrical Impedance Spectra of Dye Solar Cells Operated Under Open-Circuit Conditions. *Electrochim. Acta* **2002**, *47*, 4213−4225.

(57) Adachi, M.; Sakamoto, M.; Jiu, J.; Ogata, Y.; Isoda, S. Determination of Parameters of Electron Transport in Dye-Sensitized Solar Cells Using Electrochemical Impedance Spectroscopy. *J. Phys. Chem. B* **2006**, *110*, 13872−13880.

(58) Velusamy, M.; Hsu, Y.-C.; Lin, J. T.; Chang, C.-W.; Hsu, C.-P. 1-Alkyl-1*H*-imidazole-Based Dipolar Organic Compounds for Dye Sensitized Solar Cells. *Chem. - Asian J.* **2010**, *5*, 87−96.

(59) Chou, H.-H.; Chen, Y.-C.; Huang, H.-J.; Lee, T.-H.; Lin, J. T.; Tsai, C.; Chen, K. High Performance Dye-Sensitized Solar Cells Based on 5,6-Bis-hexyloxy-benzo-[2,1,3]thiadiazole. *J. Mater. Chem.* **2012**, *22*, 10929−10938.